Universidad Carlos III de Madrid
e-Archivo

Institutional Repository

This document is published in:

PeneloPET simulations of the Biograph ToF clinical PET scanner

K. M. Abushab, *Member, IEEE,* J. L. Herraiz, *Member, IEEE* , E. Vicente, *Member, IEEE,* S. España, *Member, IEEE,* J.J. Vaquero, *Senior Member, IEEE,* B. W. Jakoby, *Member, IEEE,* and J.M. Udías, *Member, IEEE*

Abstract–Monte Carlo simulations are widely used in positron emission tomography (PET) for optimizing detector design, acquisition protocols, as well as for developing and assessing corrections and reconstruction methods. PeneloPET is a Monte Carlo code for PET simulations which considers detector geometry, acquisition electronics and materials, and source definitions. PeneloPET is based on PENELOPE, a Monte Carlo code for the simulation of the transport in matter of electrons, positrons and photons, with energies up to 1 GeV. In this work we use PeneloPET to simulate the Biograph TruePoint (B-TP), Biograph TruePoint with TrueV (B-TPTV) and Biograph mCT PET/CT scanners. These configurations consist of three (B-TP) and four (B-TPTV and mCT) rings of 48 detector blocks. Each block comprises a 13 × 13 matrix of 4 × 4 × 20 mm^3 LSO crystals. Simulations were adjusted to reproduce some experimental results from the actual scanners and validated by comparing their predictions to further experimental results. Sensitivity, spatial resolution, noise equivalent count (NEC) rate and scatter fraction (SF) were estimated. The simulations were then employed to estimate the optimum values of system parameters, such as energy and time coincidence windows and to assess the effect of system modifications (such as number of rings) on performance.

K. M. Abushab, E. Vicente and J. M. Udias are with the Grupo de Física Nuclear, Dpto. Física Atómica, Molecular y Nuclear, Universidad Complutense de Madrid, Spain (telephone: +34 91 394 4484, email: khaled@nuclear.fis.ucm.es).

J.L. Herraiz was with the Grupo de Física Nuclear, Universidad Complutense de Madrid, Spain. He is now with M+Vision Madrid MIT consortium.

E. Vicente is also with Instituto de Estructura de la Materia, Consejo Superior de Investigaciones Científicas (CSIC), Madrid, Spain.

S. España was with the Grupo de Física Nuclear, Universidad Complutense de Madrid, Spain. He is now with the Department of Electronics and Information Systems, MEDISIP, Ghent University IBBT IBiTech, De Pintelaan 185 block B, B 9000 Ghent, Belgium (S. España e mail: samuel@nuclear.fis.ucm.es).

J. J. Vaquero is with Departamento de Bioingeniería e Ingeniería Aeroespacial, Universidad Carlos III de Madrid, Spain and with the Unidad de Medicina y Cirugía Experimental, Hospital General Universitario Gregorio Marañón, Madrid, Spain (J.J. Vaquero e mail: juanjose.vaquero@uc3m.es).

B. W. Jakoby is with Siemens Medical Solution USA, Inc., Knoxville, TN, USA, and also with the Univ. of surrey, Guildford, Surrey, UK, and Univ. of TN Medical Center, Knoxville, TN, US (B. W. Jakoby e mail: bjoern.jakoby@siemens.com).

I. INTRODUCTION

Many commercial PET scanners include time-of-flight (TOF) capability, which allows measuring the difference in arrival times between the two gamma rays of each coincidence event [1]. TOF information reduces noise and unwanted counts in the reconstructed images [2], [3]. There are unavoidable tradeoffs when choosing the characteristics of a PET scanner. For instance, by increasing the length of the scintillator crystal, the sensitivity of the scanner improves but spatial resolution diminishes due to depth-of-interaction (DOI) effects [4]. Increasing the number of detector rings improves sensitivity, but also the complexity and cost of the PET scanner. Therefore, the selection of parameters should be carried out carefully. Accurate, validated simulation tools are of invaluable help for this purpose. Indeed, Monte Carlo simulations are widely used in PET to optimize detector design and acquisition protocols [5], [6], and for developing and assessing corrections and reconstruction methods [7], [8]. Monte Carlo methods make it possible to estimate scanner properties which cannot be easily determined experimentally, as well as to assess the change in performance of PET scanners induced by modifications in scanner characteristics [9]. In recent years, the availability of powerful computers facilitated widespread use of PET-dedicated simulation codes [10], [11], and [12].

PeneloPET [13] is a Monte Carlo code based on PENELOPE [14], [15], which allows for fast and easy simulation of PET scanners. Its basic components are detector geometry and materials, acquisition electronics, and source definitions. All these components are defined in a few plain text input files [13]. PeneloPET simulations can easily be performed in a cluster of computers.

In this work, acquisitions of the Biograph TruePoint (B-TP), Biograph TruePoint with TrueV (B-TPTV) and Biograph mCT PET/CT scanners [16], [17] were simulated with PeneloPET. When simulating an existing scanner, it may be the case that not every parameter of the scanner is known with complete certainty. Often, details of the geometry, materials, acquisition electronics or the processing chain of coincidences are not available. In the first part of this work we employ the published values [16] for sensitivity, noise equivalent count (NEC) rate, and TOF capabilities of the B-TPTV scanner to optimize the simulations. Once all the parameters of the scanner needed for the simulations have been determined this

way, further results of the simulations, such as scatter fraction and spatial resolution were compared with published experimental results for the B-TPTV scanner. As further validation, predictions of sensitivity, NEC and scatter fraction for the B-TP and mCT scanners were compared to the published measurements. And finally, once the simulations have been setup and validated, they have been used to study the effect of varying parameters, such as crystal length, number of detector rings, energy resolution, coincidence time and energy windows, on the performance of Biograph scanners.

II. MATRERIALES AND METHODS

The Biograph PET/CT scanners investigated in this work consist of three (B-TP) and four (B-TPTV and mCT) rings of 48 detector blocks. Each block comprises a 13×13 matrix of $4 \times 4 \times 20$ mm³ LSO crystals. The B-TP covers an axial field-of-view (FOV) of 16.2 cm, whereas the B-TPTV extends the axial FOV to 21.8 cm. Both scanners operate in 3-dimensional (3D) mode [16], with a maximum ring difference of 38 and 27 respectively. The Biograph mCT PET scanner [17] is essentially based on the same geometry as the B-TPTV but acquires data with an extended ring difference of 49. Table I shows the characterizations of the scanners used in this study.

TABLE I. CHARACTERISTICS OF THE PET SCANNERS EVALUATED

Number of block rings	Axial FOV [cm]	Maximum ring difference
B TP	16.2	27
B TPTV	21.8	38
mCT	21.8	49
5 rings	27.2	38
8 rings	43.6	38
10 rings	54.5	38

The NEMA NU 2-2007 protocol [18] was followed in order to investigate line source sensitivity, count rate behaviour and, for the B-TPTV scanner, also spatial resolution. In addition, TOF capabilities of the scanner were also explored in the simulations. Further, configurations of scanners with 5, 8 and 10 rings, with a maximum ring difference of 38, were also simulated in order to assess the performance benefit of using larger scanners. A sketch of the scanner geometries is shown in Fig. 1.

A. Sensitivity

The sensitivity of a PET scanner represents its ability to detect 511 keV photons resulting from positron annihilation, with respect to the number of emitted positrons. PeneloPET simulations were performed to estimate the system sensitivity, following the NEMA protocol [18]. A 70 cm long polyethylene tube with an inner diameter of 1 mm was activated with about 3.9 MBq of [18]F. This activity is low enough to assure that dead time losses were less than 1% and

that the ratio of random to true events was less than 5%. The sensitivity at two transaxial positions (0 and 10 cm) was obtained. Simulations accumulated more than 10^6 detected events at each position. The simulations employed with maximum ring difference (27 and 38 for B-TP and B-TPTV respectively, and 49 for mCT) as in the acquisitions of the real scanners [16], [17].
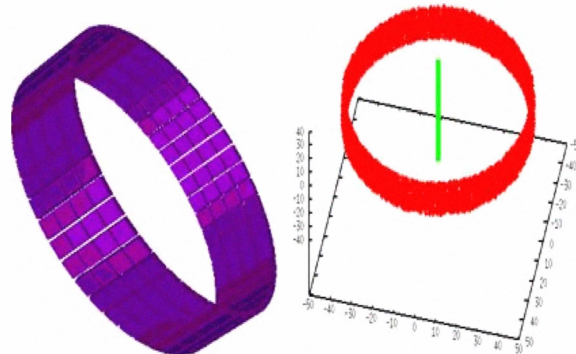

Fig. 1. PeneloPET geometry of the Biograph scanner (B TPTV), left: detector modules; right: sample source emissions (green points) and interactions of the emitted photons with the detector crystals (red points).

B. Scatter Fraction (SF) and Noise Equivalent Count (NEC) Rate

The fraction of coincidences that have scattered and yet are acquired within the applied energy window is known as scatter fraction (SF) [19]. Scatter counts decrease image contrast, just like random counts. Following the NU 2-2007 protocol, the scatter fraction was measured from low activity simulations, where random counts are negligible [18]. Another important parameter of a PET scanner is the NEC rate. NEC is a global measure, taking into account scatter and random coincidences, of the scanner ability to acquire useful counts. The NEC rate is defined as [20]:

$$NEC = \frac{T^2}{T+S+R} \qquad (1)$$

where T is the true coincidence count rate, S is the count rate of scatter coincidences and R is the count rate of random coincidences falling within the boundary of the object. The NEC has been shown to be proportional to the square of the signal-to-noise ratio [20], [21], [22] where the signal refers to the true events and the noise to the combined statistical fluctuations from all types of events. NEC is plotted as a function of activity concentrations. The peak of the NEC curve depends on geometry, scanner materials, energy windows, and acquisition electronics, mainly dead time and coincidence time window.

In this work, the simulated NEC curve for the Biograph scanners was obtained after simulating acquisitions which followed the NEMA NU 2-2007 [18] protocol to measure NEC and SF. Thus, acquisitions of a 70 cm long and 20 cm diameter polyethylene cylinder positioned with its isocenter in the isocenter of the FOV of the scanner were simulated. A line source was activated with 1.04 GBq of ^{18}F and inserted

axially into the cylinder hole, located 4.5 cm below the central phantom axis. Data were simulated for 35 frames, spanning 10 hours of acquisition.

PeneloPET allows for different independent dead time sources. There is a *singles* dead time, which applies to every photon that reaches the scanner detectors. Further there is also a *coincidences* dead time, representing the dead time involved in the processing of events identified as coincidences. Also, integration time, pile-up (and pile-up rejection) effects [13] are also included in PeneloPET. In order to mimic the behaviour of a real PET scanner, where the full details of the electronics may not be known or either are too complex, we use the parameters which define the acquisition electronics in PeneloPET as effective fitting variables adjusted to reproduce the experimental random counts, prompt counts and NEC curves of the B-TPTV scanner. Well known parameters of the scanner, such as coincidence time and energy window were set to the actual values of the real scanner [16].

C. Spatial resolution

The spatial resolution of a PET scanner represents its ability to disentangle two close point sources and it is usually characterized by the width of the reconstructed point spread function of point sources. Again, the NEMA NU 2-2007 [18] protocol was followed to determine the resolution from simulated acquisitions; an ^{18}F activated point source with low activity in a glass capillary was modelled. The activity was low enough to assure a ratio of random to total events below 5% [23]. Simulated data were acquired at two axial positions (center of the axial FOV and 1/4 off-center), at three *(x, y)* locations: (0, 1 cm), (10 cm, 0), and (0, 10 cm). The acquisition time was long enough so that at least one hundred thousand counts were acquired for each position. Filtered back projection (with ramp filter) was used to reconstruct the acquired sinogram data into 336 × 336 × 109 voxels images (voxel size: 2 × 2 × 2 mm^3). The point spread function images were obtained without attenuation and scatter correction, and no post-smoothing filter was applied.

D. Time-of-flight (TOF)

TOF in a PET scanner refers to the capability of measuring the difference in detector arrival times between the detection of the two coincidence photons ($\Delta t = t_1 - t_2$). TOF information helps to better locate the annihilation point of the emitted positron along the line of response (LOR) that connects the two opposite detectors. The distance Δx of the annihilation point from the center of the (LOR) (Fig. 2) is related to the time difference Δt by:

$$\Delta x = \Delta t \times c / 2 \qquad (2)$$

where c is the speed of light.

The system TOF resolution ($\delta(\Delta t)$ in Fig. 2) of the scanner is defined as the Full-Width-at-Half-Maximum (Δt_{FWHM}) of the distribution of time differences collected from a centered point source.

According to Eq. 2, in order to achieve a spatial resolution better than 1 cm, a TOF resolution of 66 picoseconds would be required. In many commercial scanners, the TOF resolution is of the order of 1 ns [2]. However, modern PET/CT scanners have obtained TOF resolutions of the order of 500 ps, which offer the opportunity of using TOF information to improve the quality of the reconstructed images [24]. Indeed, employing TOF information, image background, which is essentially noise, can be reduced. We may expect a system time resolution of around 550 ps for LSO based systems [25]. Time difference distributions were obtained from a 3.9 MBq of ^{18}F point source located at the center of the scanner. These distributions were fit to a Gaussian plus a background of random coincidences. The FWHM of the Gaussian was used as a measure of the TOF resolution.
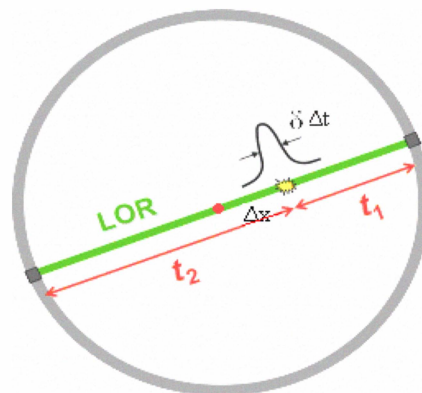

Fig. 2. Principle of TOF for an off centered annihilation

E. Impact of the Characteristics of the Scintillator Crystal and Coincidence Time Window on the Scanner Performance

Two scanner parameters which could affect sensitivity were studied: crystal length and crystal energy resolution. The relationship between crystal length and sensitivity was investigated via simulations using crystals with an axial length from 2.0 cm to 9.5 cm. Increasing the crystal length to 3 cm will result in a sensitivity gain of 1.4 [11]. Furthermore, sensitivity as a function of energy resolution in the range of 10% - 50% was studied. In addition, several values for the lower energy level discriminator (LLD) were simulated with a constant value of 650 keV for the higher level energy discriminator. It is well known that the scatter fraction may decrease by increasing the LLD [26]. We assessed the effect of the LLD on both NEC and SF.

Coincidence events require that both photons from positron annihilation are detected by the system electronics within a certain time window. The acquisition electronics has to allow for a coincidence time window large enough to cover for the actual TOF required for a photon to reach the detector ring. However, a too large coincidence time window may result in an increase of random coincidences. Therefore, the optimal choice of time coincidence window which yielded the maximum NEC was investigated. For this purpose,

acquisitions with coincidence time windows of 4, 4.5, 5, 6 and 7 ns were considered. Other than for this study, a default 4.5 ns coincidence time window was employed for all other simulations in this work.

F. Impact of the Number of Detector Rings on the Scanner Performance

The dependence of the sensitivity, NEC rate and SF on the number of block detector rings was explored. Variations of the Biograph PET scanner with the same geometry and characteristics but with additional block detector rings (from 3 to 10) were considered. A maximum ring difference of 38 was used for all scanners, except for the B-TP and mCT, for which a maximum ring difference of 27 and 49 was employed respectively. The simulations would yield and estimation of the increase in sensitivity and count rate performance obtained with additional detector rings as well as with the increase of the maximum ring difference.

G. Uncertainty estimates

When simulating existing PET systems, uncertainties due to statistical fluctuations can be reduced to a level of insignificance by running the simulation with a large number of events. In addition, the existing physics models within PENELOPE [14], [15] have been validated against experimental data and are therefore not a significant source of uncertainties. Thus, simulated predictions can be obtained, which are within a few percent of the experimental results of the PET scanners [13]. The main source of uncertainty in the simulation is the lack of precise knowledge of all parameters of the real scanners. It may be, for example, that the detailed scanner geometry is not fully known. Exact information about the scanner geometry and the materials of the scanner, such as the bed, shielding and covers are not fully known. Most often, only general geometry details and some performance results are available for commercial scanners. The same applies to the internal electronics and count processing chain. Thus, it is necessary to use simulations flexible enough to include parameters that can be optimized to reproduce the experimentally obtained performance results. In the case of the Biograph scanners, we have chosen the following performance measurements to optimize the simulations:

1. *Sensitivity*. The measured sensitivity values for the B-TPTV scanner were taken as a reference. PeneloPET simulations, which employ the basic geometry definitions for this scanner (radius, block size, crystal dimensions) and assume no reflector in between crystals, overestimate sensitivity by 12% (see Table II). This could be due to a series of causes, for instance the radius of the actual scanner may be 4-5% larger than assumed, or there may be a small amount of reflector in

between scintillator crystals. We have chosen to include a reflector, which is thick (0.4 mm) enough to reproduce the B-TPTV sensitivity. We make no claim that this simulation result implies that there is any amount of reflector in the real system, but rather consider this as an effective way of taking into account the bulk of unknown geometry parameters in the scanner performance. The measured sensitivity values include uncertainties in the order of 5%, which mostly originate from the source activities employed in the measurements [16], and therefore these uncertainties are translated into the sensitivity predictions of the simulations. Other predictions that depend mainly on the geometry of the scanner, such as scatter fraction, include similar uncertainties. The comparison with measured results for other scanners supports this estimate.

2. *Count rate* as a function of activity concentration curves. Reproducing the experimental behaviour of the system would require detailed knowledge of the acquisition electronics. Instead, we have taken the trues, randoms and NEC rates as a function of activity concentration curves for the B-TPTV scanner as a reference. A 5% source uncertainty was included. In order to avoid regions in which additional bottlenecks in the processing of events by the real scanners may arise, we focus on count rates below the peak of the NEC, where we ensured that deviations of the simulations from the real B-TPTV system remained below 10%. We thus estimate the deviations of the predictions of the simulations for all other Biograph systems should remain below 10%, for count rates smaller than the NEC peak.

III. RESULTS AND DISCUSSION

A. Sensitivity

The experimental and simulated sensitivity results of the B-TPTV scanner are listed in Table II. It must be noted that the available information about the scanner geometry (B-TPTV) lacks some details to completely set up the simulations. In particular, the actual thickness of the inter-crystal reflector is not known. Simulations without crystal reflector would overestimate the experimental sensitivity quoted by [16] by 12%. The use of a reflector thickness of the order of 0.4 mm yields good agreement with the measured sensitivity at several distances to the axis of the scanner. Indeed, an average sensitivity of 8.2 kcps, both at 0 and 10 cm off-center, was

TABLE II. SUMMARY OF VALUES FOR SENSITIVITY, NEC, AND SF FOR DIFFERENT SCANNER CONFIGURATIONS, ACCORDING TO SIMULATIONS. IN BOLDFACE ARE SHOWN THE RESULTS THAT WERE EMPLOYED TO FIX SOME SCANNER PARAMETERS IN THE SIMULATIONS. ALL RESULTS ARE OBTAINED WITH A TIME COINCIDENCE WINDOW AND AN ENERGY WINDOW SAME AS THE MEASURED. EXPERIMENTAL RESULTS ARE TAKEN FROM [16], [17]

Number of block rings	NEC [Kcps] @[kBq/ml]			Scatter fraction [%]			Sensitivity [kcps/MBq] @ 0 and 10cm off center		
	Simulated (this work)	Simulated [11]	Experimental	Simulated (this work)	Simulated [11]	Experimental	Simulated (this work)	Simulated [11]	Experimental
B TP	90 @ 33	100@34	93@34	34.3	33	32.0	4.6	4.8	4.5
B TPTV	**161@32.5**	177@34	161@31.5	31.3	35	32.5	w/o reflector 9.2 **with reflector 8.2**	8.7	8.2
mCT	177@34	-	180.3@29	34.8	-	33.5	9.8	-	9.7
5 rings	259@39	-	-	30.8	-	-	12.5	-	-
8 rings	489@35	-	-	32.0	-	-	31.7	-	-
10 rings	787@30	800@31	-	33.1	35	-	48.7	47.8	-

obtained with this assumption for reflector thickness, which was subsequently employed in all simulations in this work. Once this assumption is made, sensitivity of the B-TP and mCT are predicted within 2% of the experimental values. In general our simulated sensitivities for B-TP and B-TPTV are in good agreement with the measured [16] ones. Eriksson et al [11] using GATE and no reflector, obtained a sensitivity about 6% larger than the experimental values (Table. II)

B. Scatter fraction and Noise Equivalent Count Rate

Fig. 3 and Table II present the simulated and experimental results for randoms, trues and NEC rates for the B-TPTV scanner. Acquisitions according to the NEMA NU-2007 protocol for NEC measurement [18] were simulated. 4.5 ns coincidence time and a 425–650 keV energy windows, same as for the experimental systems, were employed. Parameters of the simulated electronics for data acquisition of PenelopET were adjusted so that the experimental random, trues, and NEC curve below the NEC peak were reproduced by the simulations. With this procedure, an effective representation of the behaviour of the electronics and event processing software of the real scanners should be obtained. In the simulations, a peak NECR of 161 kcps at a concentration of 32.5 kBq/ml was obtained, close to the experimental value of 161 kcps at a concentration of 31.5 kBq/ml [16]. Certainly it would have been possible to match the NEC peak vale and position of the simulations more closely to the experimental results; however one can see how at high activity concentrations, beyond approximately 33 kBq/ml, the experimental curves show a strong negative slope. This is very likely due to additional dead time losses at high count rates associated to bottlenecks in disk data storage and CPU event processing, which are not considered in the simulations. We thus fit the simulations only to experimental data below 33 kBq/ml which also in a agreement with the simulated study conducted by Eriksson et al. [11]. The simulated peak true coincidences rate of 873 kcps appears then at 46 kBq/ml, compared to a measured true peak coincidence rate of 804 Kcps at an activity concentration of 38 kBq/ml Fig. 3(a). We consider that this difference (8% in value of the peak of the true counts) between simulated and measured value of the true coincidences is a reasonable indication of the uncertainty in the simulated results for count rates versus activity curves, and it is of similar magnitude than the quoted error of 5% in the experimental activity [16]. Once the parameters of the acquisition electronics are settled from these measurements, they are employed unchanged for the other scanners analyzed in this work: BTP and mCT scanners and 5, 8 and 10 ring scanners. The differences between the simulated NEC peak values and the experimental ones are less than 3% for both BTP and mCT scanners. For the position of the NEC peak, a difference of 3% is observed for BTP and 15% for the mCT. This may be considered as a measure of the reliability of simulations for these performance figures. The corresponding NEC rate curves are plotted in Fig. 3(b), along with the experimental ones.

In addition, simulations are employed to predict NEC peak values for scanners with 5, 8 and 10 rings, with a maximum ring difference of 38. They are also quoted in Table II. The peak NEC for the 10-ring system is 787 kcps at a concentration of 30 kBq/ml, in good agreement with the simulated study (800 kcps @ 31 kBq/ml) of Eriksson et al. [11]. The NEC for the 10-ring system is five time higher than the B-TPTV system. An increase in peak NEC rate and sensitivity can be observed for additional detector rings, while the scatter fraction remains fairly constant. A similar behaviour was also observed in simulations of Badawi et al. [10] using SimSET. Increasing the axial extent from 4 (B-TPTV) to 5 rings, increases the sensitivity by 40%. With an axial extent of 10 rings, which corresponds to an axial FOV of 54 cm, we observe a sensitivity gain by a factor of 6. This result is similar to that obtained by Eriksson et al. [11] with GATE. It must be recalled that a maximum ring difference of 38 was employed for these cases, which corresponds to the value used in the B-TPTV scanners. For the simulation of B-TP and mCT, the maximum ring difference was set to 27 and 49, respectively.

Another prediction of simulations that can be compared to experiment is the SF. It is independent on electronics, being influenced only by time and energy windows and scanner and source geometry. The SF is determined from simulated

acquisitions according to the NEMA NU 2007 protocol. The simulated predictions and the experimental values are within 4% (Table II). One must note that the SF is a genuine prediction of the simulations, as no parameters have been fit to reproduce it.

Overall our simulated results for SF and NEC obtained for the B-TP, B-TPTV and mCT PET systems are in fair agreement with the experimental results [16], [17].
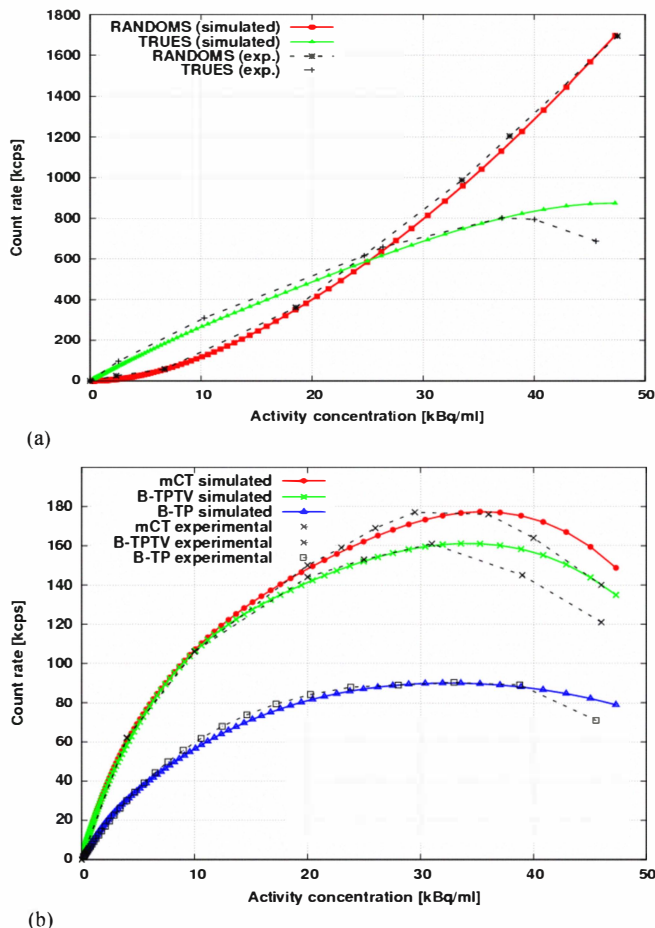

(a)

(b)

Fig. 3. Comparison of random and true rate curves as a function of activity concentration predicted by PeneloPET simulations adjusted to the experimental results of the B TPTV. The random rate curve has been multiplied by 0.4 in order to fit in the plot (a). Simulated and experimental NEC curves for the B TP, B TPTV, and mCT scanners (b). All curves have been obtained with coincidence time and energy windows same as measured [16], [17].

C. Spatial resolution

The FWHM and FWTM of the reconstructed point source images are reported in Table III. The simulated and experimental spatial resolution results of the B-TPTV scanner are compared. The simulated average spatial resolution at 1 cm and 10 cm radial off-center is 4.4 mm and 5.3 mm, respectively. It is in reasonably agreement with the results obtained experimentally of 4.4 ± 0.3 mm and 5.0 ± 0.3 mm [16]. Other values reflected in Table III are in general also in agreement with the measurements.

TABLE III. SIMULATED AND EXPERIMENTAL SPATIAL RESOLUTION FOR THE B TPTV SCANNER. EXPERIMENTAL RESULTS BEAR AN UNCERTAINTY OF ± 0.3 MM [16]

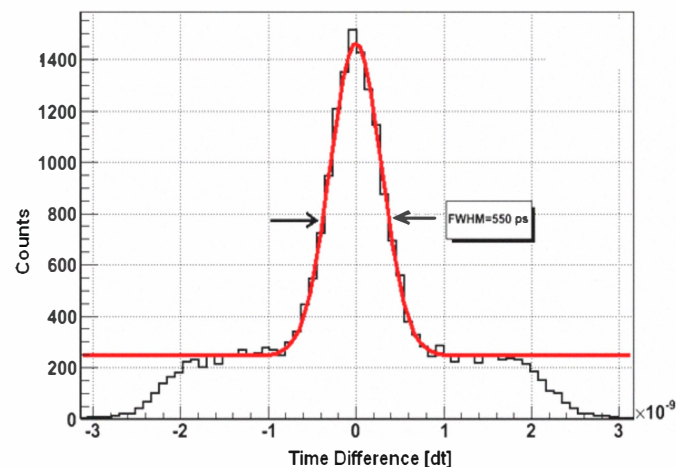|	FWHM (mm)		FWTM (mm)	
	Simulated	Experimental	Simulated	Experimental
1 cm off center				
Transverse	4.6	4.2	8.5	8.1
Axial	4.2	4.5	8.4	9.2
Average resolution	**4.4**	4.4		
10 cm off center				
Transverse radial	5.5	4.6	9.0	9.4
Transverse tangential	5.6	5.0	10.2	9.4
Axial	4.4	5.5	7.5	10.5
Average resolution	**5.3**	5.0		

Fig. 4. Gaussian fit of the simulated TOF distribution from a centered source. A rise time of 0.8 ns for the LSO crystals combined with additional jitter of 0.3 ns is employed in the simulations to produce a TOF resolution of 550 ps (FWHM) for the B TPTV scanner.

D. Time-of-Flight (TOF)

As shown in Fig. 4, simulations allow plotting time differences of arrivals of photons in the scanner. In this case, for a point source located at the center of the scanner. A peak appears on the top of a background of random events. As it was the case for the NEC, precise timing properties of the scanner depend not only on the timing properties of the scintillator but also on the electronics and post processing of events. PeneloPET has two parameters related to timing. One is the rise time of the scintillator, the other one is an additional time jitter added to the time stamp given to each event. We use the quoted timing properties of the lutetium oxyorthosilicate (LSO) scintillation crystal [27], in particular a rise time of 0.8 ns. In order to reproduce the reported TOF resolution of the Biograph scanners [28], [29], of about 550 ps FWHM, an additional jitter of 0.3 ns must be included in the simulations. These additional 0.3 ns may account for time rise or noise variation among different crystals and PMTs, or for time-lag effects in the electronics.

E. *Impact of the Characteristics of the Scintillator Crystal and Coincidence Time Window on the Scanner Performance*

The impact of varying crystal length on system sensitivity is shown in Fig. 5(a). Up to a crystal length of 3 cm, a linear relationship between sensitivity and crystal length can be observed. Beyond 3 cm, the increase of sensitivity seems to approach an asymptotical value. For the performance simulations, the same crystal length of 2 cm was used as employed in the actual scanners. With 3 cm of crystal, the gain increases by a factor of 1.5, as also seen in the simulated study of Eriksson et al [11]. The sensitivity as a function of crystal energy resolution is shown in Fig. 5(b) for the same energy window of 425 to 650 keV. For a given energy window, sensitivity is affected by the energy resolution. It can be observed that beyond an energy resolution of 20%, the sensitivity decreases linearly with increasing energy resolution. For an energy resolution of less than 20%, the sensitivity is barely affected. In our simulations, the reported energy resolution for LSO of 12% was employed [30].
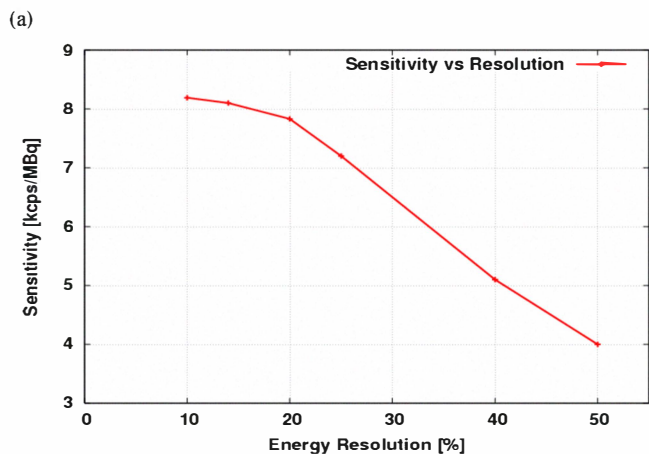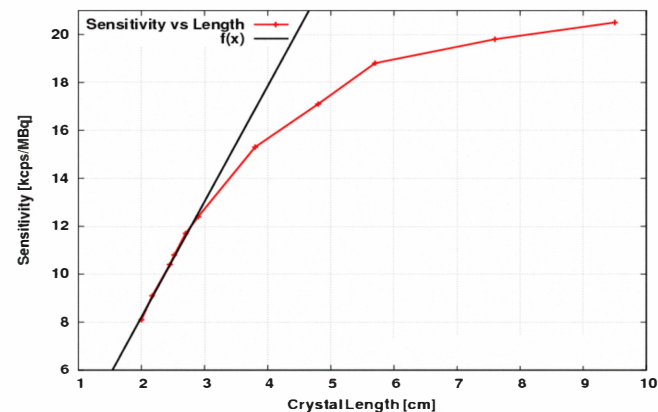

(a)

(b)

Fig. 5. Sensitivity of the B TPTV scanner as a function of the crystal length (a) and energy resolution (b) for a fixed energy window of 425 650 keV.

Table IV presents SF values for different LLDs. As expected, simulations with a wider energy window (375-650 keV) result in the highest SF while an LLD of 475 keV yields the lowest SF. These results agree with Eriksson et al [11].

Fig. 6 shows the resulting peak NEC rate for different LLDs. Less scatter events will be detected if the LLD is raised but raising it too much would also cause a loss of true events. Thus an optimal LLD value exists that maximizes the NEC. Indeed, and LLD of 425 keV, as employed in the experimental systems, appears to yield the highest peak NEC rate (see Fig. 6).

TABLE IV. SIMULATED VALUES FOR SF VS LLD FOR B TPTV

Lower level discriminator [keV]	Scatter fraction [%]
375	53.1
400	46.8
425[a]	31.3
475	23.2

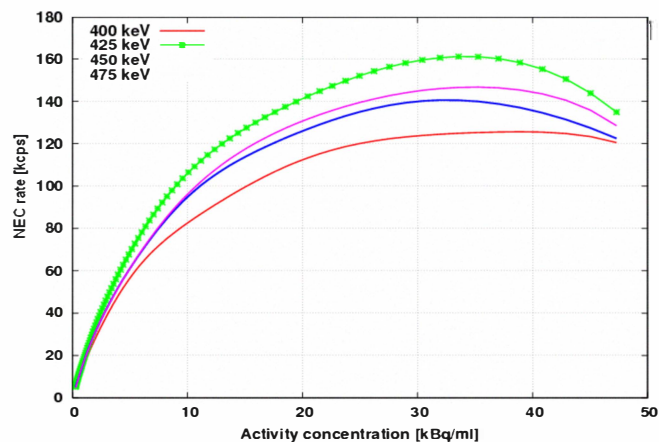[a] default value for the real scanner

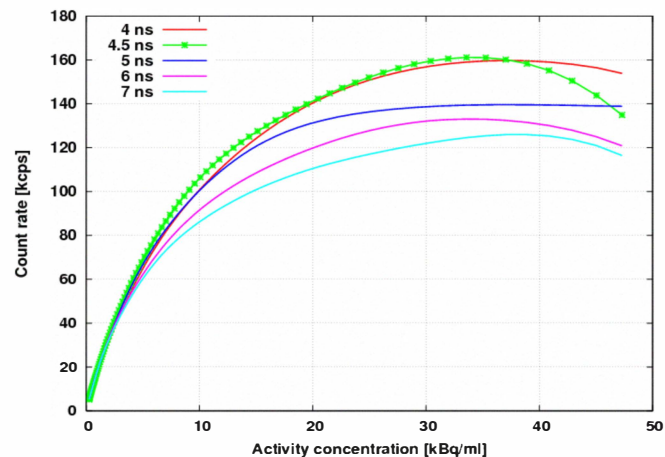Fig. 6. NEC rates as a function of the LLD for the B TPTV scanner.

Fig. 7. NEC curves with different coincidence time windows for the B TPTV scanner

With regard to coincidence time window, using too wide windows will cause an increase in random events, and therefore the NEC count rate would decrease. However, a count rate reduction would follow from the use of too narrow

coincidence time windows. Thus, again, it may be possible to obtain an optimum value of the time coincidence window. Simulated results of NEC curves for different coincidence time windows are shown in Fig. 7. 4.5 ns yields the highest peak NEC rate. This is the default value employed in the for B-TPTV scanner [16].

IV. SUMMARY AND CONCLUSIONS

The aim of this work was to assess the capability of PeneloPET to simulate clinical PET/CT systems. For this purpose, performance measurements of the B-TP, B-TPTV and mCT PET/CT scanners (Siemens Medical Solutions USA, Inc.) were simulated and the results compared with experimentally obtained data.

A reflector thickness of approximately 0.4 mm had to be included in our simulations in order to achieve the sensitivity measured on the B-TPTV. Once this parameter was selected to reproduce the experimental performance results of the B-TPTV scanner, it was not changed for the simulations. PeneloPET is flexible enough to easily accommodate different dead time ingredients in the electronics, which have been optimized so that the experimental NEC curves for the B-TPTV could be reproduced. For the NEC curves, deviations between simulated and experimental results for high activity concentrations, well beyond the peak of the NEC, were observed. This is very likely due to limitations in data storage and other factors that were not included in PeneloPET. Once the simulation was optimized to reproduce the NEC rate curves and sensitivity of the B-TPTV scanner, predictions for scatter fraction derived from the simulation (Table II), agree within 5% with the measured values for the three scanners under investigation. Furthermore, the sensitivity and NEC rate curves for both the B-TP and are also reasonably predicted. The simulated and experimental spatial resolution results were also comparable (Table III). These performance results validate the use of PeneloPET to simulate the clinical scanners. Therefore, simulations were employed to investigate the variation of several basic scanner parameters on the performance of the B-TPTV system. For example, Fig. 5(b) shows an inverse relationship between crystal energy resolution and sensitivity, for a given energy window. Furthermore, the impact of the energy window on the system sensitivity was explored, as well as the effect on the peak NEC values and SFs. Simulations allowed identifying optimal choices of coincidence time and energy windows. For the B-TPTV, the simulations confirmed that the default factory values of a 425 to 650 keV energy window and a 4.5 ns coincidence time window are optimal choices.

Many commercially available PET scanners are made of block detector rings. The sensitivity of the PET system can be increased by adding more detector rings and also by increasing the maximum accepted ring difference. The extended ring difference of the mCT PET scanner leads to a 19% increase in sensitivity compared to the B-TPTV scanner. The larger ring difference of the mCT also leads to a 10% increase of the peak NEC, compared to the B-TPTV (Table II). The simulation of MacDonald et al [31] with SimSET also agrees with the observed increase of sensitivity and NEC with increasing axial FOV and maximum ring difference predicted by PeneloPET.

We have shown that PeneloPET is suitable for simulating and investigating clinical systems. The Biograph TruePoint, TruePoint with TrueV and mCT PET/CT systems were simulated successfully. Good agreements were obtained between simulated and measured results, and with results of other simulations. The reliability of our Monte Carlo code was thus validated. PeneloPET simulations allowed studying the impact of different acquisition parameters and scanner geometries on the overall system performance. Furthermore, we have shown that PeneloPET is capable of incorporating TOF properties of modern scanners. With the help of these simulations, the impact of TOF on the image quality will be our goal for future investigations.

REFERENCES

[1] T. K. Lewellen, "Time of flight PET," *Seminars. Nucl. Med.* vol. 28, no. 3, pp. 268 275, 2006.
[2] W. W. Mouses "Time of flight in PET Revisited," *IEEE Transactions on Nuclear Science*, vol. 50, no. 5, pp. 1325 1330, 2003.
[3] M. Conti "Why is TOF PET reconstruction a more robust method in the presence of inconsistent data?" *Physics in Medicine and Biology*, vol. 56, pp. 155 168, 2011.
[4] W. D. Kunze, M. Baehre and E. Richter, "PET with a Dual Head coincidence camera: spatial resolution, scatter fraction, and sensitivity," *J. Nucl. Med.*, vol. 41, no. 6, pp. 1067 1074, 1999.
[5] A. Braem et al "Feasibility of a novel design of high resolution parallax free Compton enhanced PET scanner dedicated to brain research," *Phys. Med. Biol.*, vol. 49, pp. 254 2562, 2004.
[6] U. Heinrichs, U. Pietrzyk and K. Ziemons, "Design optimization of the PMT ClearPET prototypes based on simulation studies with GEANT3," *IEEE Trans. Nucl. Sci.*, vol. 50, pp. 1428 1432, 2003.
[7] I. Buvat and I. Castiglioni, "Monte Carlo simulations in SPET and PET," *The Quarterly Journal of Nuclear Medicine*, vol. 46, pp 48 61, 2002.
[8] J. L. Herraiz, S. España, J. J. Vaquero, M. Desco and J .M. Udias, "FIRST: fast iterative reconstruction software for (PET) tomography," *Phys. Med. Biol.*, vol. 51, pp. 4547 4565, 2006.
[9] H. Zaidi, "Relevance of accurate Monte Carlo modelling in nuclear medical imaging," *Medical Physics*, vol. 26, pp 574 608, 1999.
[10] R. D. Badawi, S. G. Kohlmyer, R. L. Harrison, S. D. Vannoy, and T. K. Lewellen, "The effect of camera geometry on singles flux scatter fraction and trues and randoms sensitivity for cylindrical 3D PET a

simulation study," *IEEE Trans. Nucl. Sci.*, vol. 47, no. 3, pp. 1228 1232, 2000.

[11] L. Eriksson, et al., "An investigation of sensitivity limits in PET scanners," *Nuclear instruments and methods in physics research*, vol. A 850, pp. 836 842, 2007.

[12] C. Ross Schmidtlein et al, "Validation of GEAT Monte Carlo simulation of the GE advance/discoveryLS PET scanner," Med. Phys., vol. 33, no. 1, pp. 198 208, 2005.

[13] E. España, J. L. Herraiz, E. Vicente, J. J. Vaquero, M. Desco and J .M. Udias "PeneloPET, a Monte Carlo PET simulation toolkit based on PENELOPE: Features and validation," *Phys. Med. Biol.*, vol. 54, no. 6, pp. 1723 1742, Mar. 2009

[14] F. Salvat, J. M. Fernández Varea and J. Sempau, "PENELOPE 2006: A Code System for Monte Carlo Simulation of Electron and Photon," *Transport. Nuclear Energy Agency* (NEA`6222), Barcelona, Spain, 2006.

[15] J. Sempau and P. Andrewo "Configuration of the electron transport alogarthim of PENELOPE to simulate ion chamber," *Physics in medicine and biology*, vol. 51, pp 3533 3348, 2006.

[16] B .W. Jakoby, M. Y. Bercier, C. C. Watson, V. Rappoport, B. Bendriem, D. W. Townsend, "Performance characteristics of a new LSO PET/CT scanner with extended axial field of view and PSF reconstruction," *IEEE Trans. Nucl. Sci.*, vol. 56, pp. 633 639, 2009.

[17] B. W. Jakoby, Y. Bercier, M. Conty, M. E. Casey, B. Bendriem, and D. W. Townsend "Physical and clinical performance of the mCT time of flight PET/CT scanner" *Physics of Medicine and Biology*, vol. 56, pp. 2375 2389, 2011.

[18] "Performance Measurement Positron Emission TomographS" National Electrical Manufactories Association, Rosslyn, VA, *NEMA Standards publication N2-2007*, 2007.

[19] D. L. Bailey, J. S. Karp, S. Surti, *Positron emission tomography: basic sciences.* London: Springer, 2003.

[20] S. C. Strother, M. E. Casey and E. J. Hoffman, "Measuring PET scanner sensitivity: relating count rates to image signaltonoise ratios using noise equivalent counts" *IEEE Trans. Nucl. Sci.* vol. 37, pp. 783 888, 1990.

[21] W. Worstell, H. Kudrolli, J. Nevin, R. Rohatgi, and L. Romanov, "Diversity combining signal processing and NEC in List Mode PET," *IEEE Trans. Nucl. Sci.*, vol. 7, pp. 3814 3818, 2004.

[22] S. Surti, S. J. Karp, G. Muehllehner and P. S. Raby, "Investigation of lanthanum scintillators for 3 D PET ," *IEEE Trans. Nucl. Sci.*, vol. 50, pp. 348 354, 2003.

[23] C. C. Watson, M. M. Casey, T. Beyer, T. Bruckbauer,D. W. Townsend, and D.A. Brasse, "Evaluation of clinical PET count rate performance," *IEEE Trans. Nucl. Sci.*, vol. 50, pp. 1379 1385, 2003.

[24] M. Conti, B. Bendriem, M.E. Casey, M. Chen, F. Kehren, C. Micle and V. Panin , "First experimental results of time of flight reconstruction on an LSO PET scanner," *Phys. Med. Biol.* vol. 50 , p. 4507 4526, 2005.

[25] W. W. Moses, M. Uilisch "Factors influencing timing resolution in a commercial LSO PET camera," *IEEE Trans. Nucl. Sci.*, vol. 53, no. 1, pp. 78 85, 2004.

[26] J. P. J. Carney, D. W. Townsend, "Clinical count rate performance of an LSO PET/CTscanner utilizing a new front end electronics architecture with sub nanosecond intrinsic timing resolution, "*Radiation Physics and Chemistry* , vol. 75, pp. 2182 2185. 2006.

[27] D. J. Herbert, S. Moehrs, N. D'Ascenzo, N. Belcari, A. Del Guerra, F. Morsani, V. Saveliev, "The Silicon photomultiplier for application to high resolution positron emission tomography," *Nuclear instruments and methods in physics research*, vol. A 573, pp. 84 87, 2007.

[28] D. J. Kadrmas, M. E. Casey, M. Conti, B. J. Jakoby, C. Loise, D. W. Townsend, "Impact of Time Flight on PET Tumor detection," *J. Nucl. Med.*, vol. 50, pp. 1315 1323, 2009.

[29] C. Loise et al. "An assessment of the impact of incorporating Time of Flight information into clinical PET/CT imaging," *J. Nucl. Med.*, vol. 51 237 45, 2010.

[30] B. Pichler, E. Lorenz, R. Mirzonyan, W. Pimpl, F. Roder, M. Schwaiger and S. I. Ziegler, "Performance test of a LSO APD PET module in 9.4 tesla magnet," *IEEE Nuclear science symposium*, vol. 2, pp. 1237 1239, 1997.

[31] L. R. MacDonald et al., "Measurment of count rate performance of the discovery STE PET/CT scanner in 2D, 3D and partial collimation acquisition modes," *Phys. Med. Biol.*, vol. 53, no. 14, pp. 3723 3738, 2008.